Current Continuity in Auroral System Science: Defining a Catalog of Auroral GEMINI Simulations

J. van Irsel[1] (Jules.van.Irsel.gr@Dartmouth.edu), A. Mule[1], M. Burleigh[2], S. R. Kaeppler[3], M. D. Zettergren[4], K. A. Lynch[1]; SA31B-2857

[1]Dept. of Physics & Astronomy, Dartmouth College; [2]Space Science Division, Naval Research Laboratory; [3]Dept. of Physics & Astronomy, Clemson University; [4]Physical Sciences Dept., Embry-Riddle Aeronautical University

Background

- Local auroral coupling of the ionosphere and magnetosphere (MI) is an open area of study (Wolf, 1975; Cowley, 2000; Khazanov et al., 2008; Lynch et al., 2022).
- MI coupling demands self-consistent, topside maps of field-aligned current (FAC) and $\mathbf{E} \times \mathbf{B}$ plasma flow that agree with ionospheric conductivity patterns created by charged particle, auroral precipitation.
- Discrete auroral precipitation provided by the auroral acceleration region creates arc-scale morphology in the ionospheric conductivity volume to which the MI coupling is highly sensitive.
- Quasi-static ionospheric plasma flow, FAC, and conductivity have a 2D topside relation given by Eq. 6.12 in Kelley (2009):

$$j_\parallel(x, y) = \Sigma_P \nabla \cdot \mathbf{E} + \mathbf{E} \cdot \nabla \Sigma_P + (\mathbf{E} \times \mathbf{b}) \cdot \nabla \Sigma_H \quad (1)$$

where $j_\parallel$ is a horizontal map of FAC at the topside ionosphere, Σ_P and Σ_H being the height-integrated Pedersen and Hall conductivities, and $\mathbf{E}$ is the perpendicular ionospheric electric field.
- For sheet-like arcs (arcs that are latitudinally narrow, longitudinally aligned, with no along-arc gradients) finding self-consistent solutions to this is relatively well-posed (Marghitu, 2012).
- This 2D picture can significantly hide the 3D nature of auroral current closure.
- Due to limitations of auroral system experiments in 3D, or even 2D, 3D data driven auroral simulations are rare.

Problem Statement

- We want to find **physical**, **self-consistent** solutions to the ionospheric **current continuity** equation using 3D modelling for less idealized discrete auroral arc systems.
- Measurements of auroral arc systems are often **sparse**, **heterogeneous**, and **distributed**, yet ionospheric models often require continuous, 2D input drivers.
- This work outlines methods for creating 2D electrostatic, **continuous** topside **boundary conditions** from distributed data provided by all-sky, multi-spectral imagery and in situ data from either spacecraft or sounding rockets.
- These boundary conditions are used to drive and assess 3D, electrostatic auroral ionospheric simulations.

Approach

- Three steps are taken to develop 2D electric potential boundary conditions:
  1. Multi-spectral, all-sky imagery proxies characteristic energy, E_0, and total precipitating energy flux, Q, with which **two arc boundaries** are determined.
  2. A single cut of in situ plasma flow data is **replicated**, **rotated**, and **scaled** in accordance with these arc boundaries.
  3. The replicated flow vectors are interpolated, and, to ensure **electrostatics** (due to model requirements), an electric potential map is found that best agrees with this continuous flow map via:

$$\mathbf{v} = \mathbf{E} \times B/B^2 = -\nabla \phi \times \mathbf{B}/B^2 \quad (2)$$

- This work improves on a similar methodology from Clayton et al. (2019, 2021) by
  A. Rotating the flow to be tangent to the primary arc boundary, and
  B. Scaling along the replicated trajectories to match shorting electric fields with regions of similarly high conductances.
- We use PFRR-DASC imagery (optics.gi.alaska.edu/optics) and plasma flow data from the Isinglass sounding rocket campaign (PI: K. A. Lynch).
- This differs from the Lompe code (Laundal et al. (2022)) in that we use quantitative information from multi-spectral, all-sky imagery to expand on limited flow data.
- Compared to work done by Nicolls et al. (2014), our electrostatic retains sharp across-arc gradients, as opposed to penalizing gradients in all directions.

The GEMINI Model

- We use multi-fluid model runs provided by GEMINI (Zettergren & Semeter, 2012; Zettergren & Snively, 2019). For details see github.com/gemini3d.
- This model is state-of-the-art and can simulate the ionosphere at auroral arc scales (see Figure 1 for context).
- GEMINI solves for static current continuity to account for changes in model parameters impacting conductivities as it steps forward in time.
- It is driven with topside precipitation maps of energy flux, Q, and characteristic energy, E_0, covering impact ionization via calculations outlined by Fang et al. (2008).
- Additionally, the model is forced at the topside with either a map of FAC or plasma flow. The simulations done in this work are all flow driven.
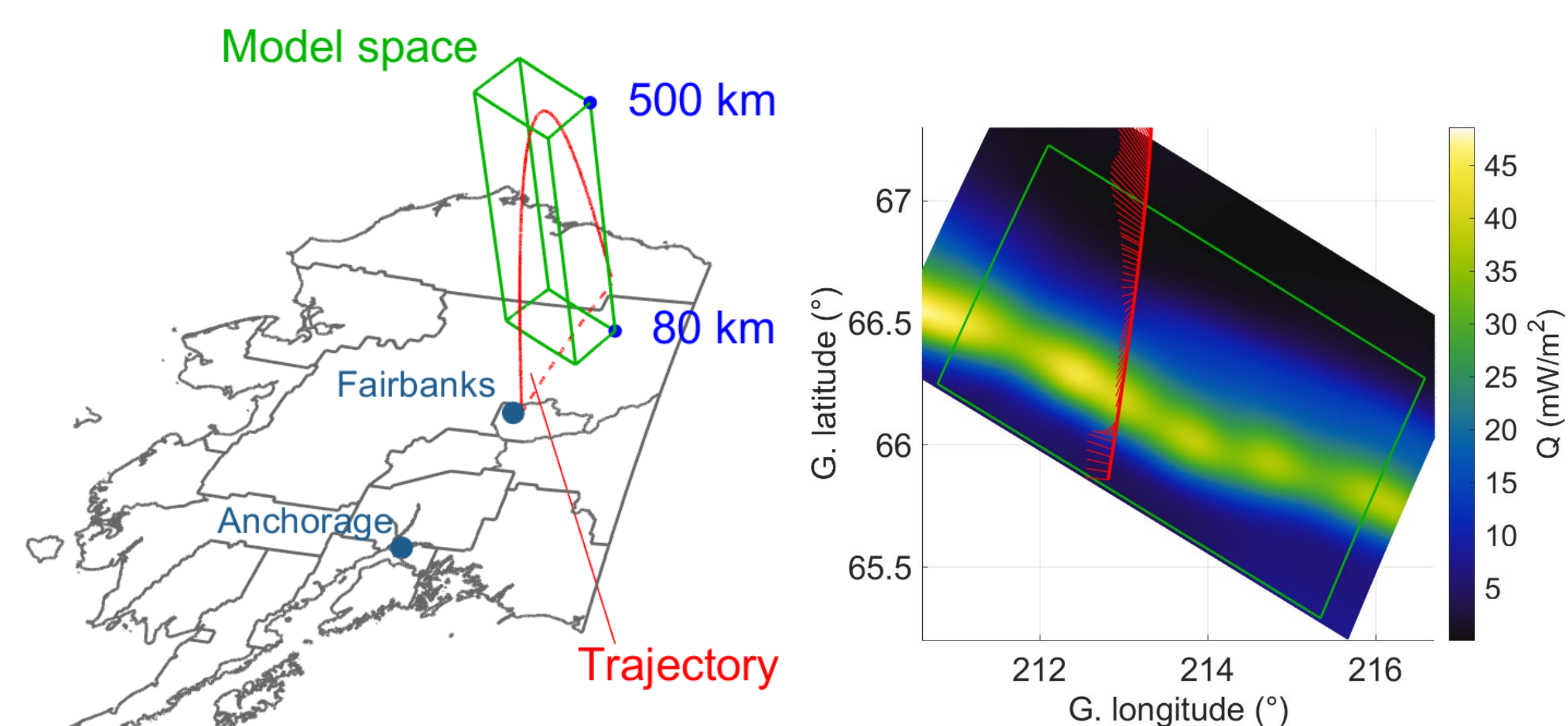
Figure 1: Context of this work. Left: The GEMINI model space used (green) and the Isinglass trajectory (red) in reference to Alaska. Right: All-sky imagery and flow data in reference to the model space.

Arc Boundary Definitions

- Boundaries are determined with either energy flux, Q, or Pedersen conductance, Σ_P.
- In this proof-of-concept, a proxy for Σ_P is made using Eq. (3) by Robinson et al. (1987), however using multi/two stream transport models (e.g. Solomon, 2017) to model conductances is recommended and will be done in future work.
- A primary and secondary boundary are determined in one of two ways (see Figure 2):
  1. Finding the first two most prominent edges at every longitude using standard Sobel edge detection (Sobel, 2014).
  2. Following two contour lines from the locations of steepest along-track gradients.
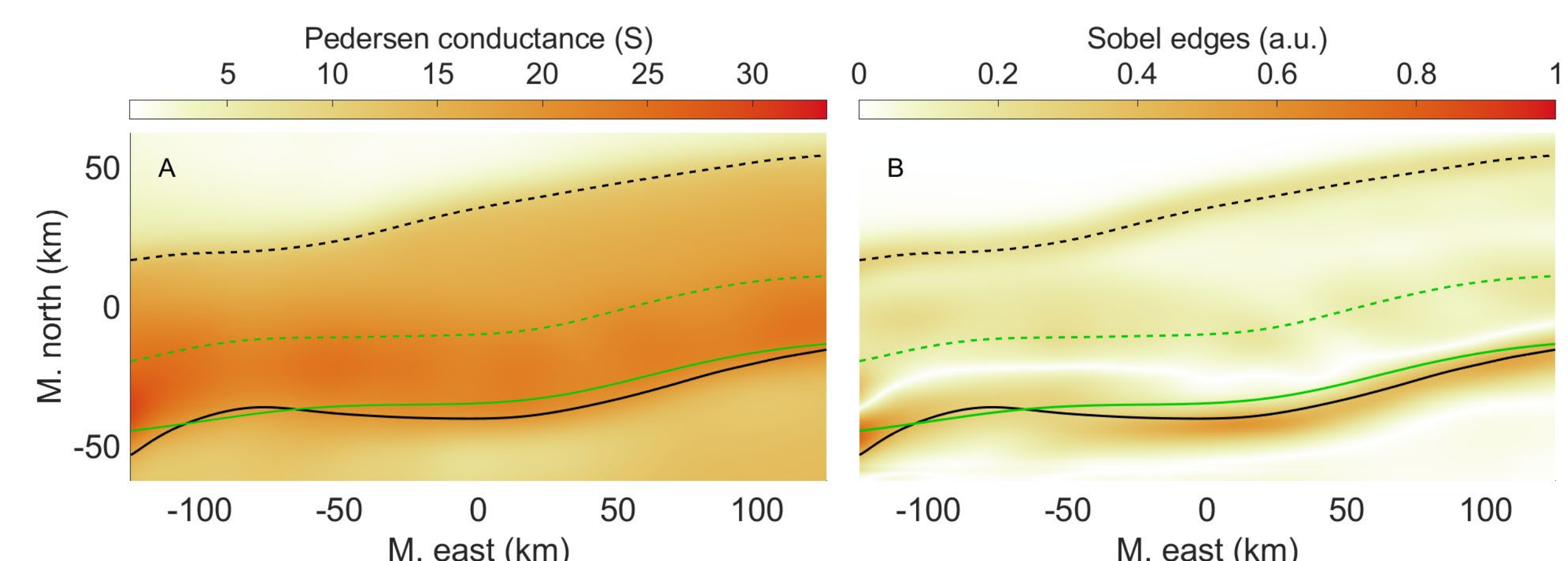
Figure 2: Primary (solid) and secondary (dashed) boundaries using Pedersen conductance and contour lines at 19.1 S and 10.5 S (black). In green are the boundaries determined using the energy flux (not shown) with the steepest gradient method. A: Pedersen conductance. B: Sobel convolution of the Pedersen conductance. Both sets of boundaries have an approximate smoothing window of 15 km.

In Situ Data Replication

- A constant background flow is removed such that the flow is tangent to the primary arc boundary when intersecting it, leaving only the arc disturbed flow to work with.
- To first order, $\mathbf{v}$ is along-arc (Marghitu, 2012) and we expect the electric field to quench inside the band of enhanced conductance.
- This is why we replicate the flow data along the arc boundaries, while remaining tangent to it, and scaling such that the shorted out electric fields remain collocated with enhanced conductance (see Figure 3).
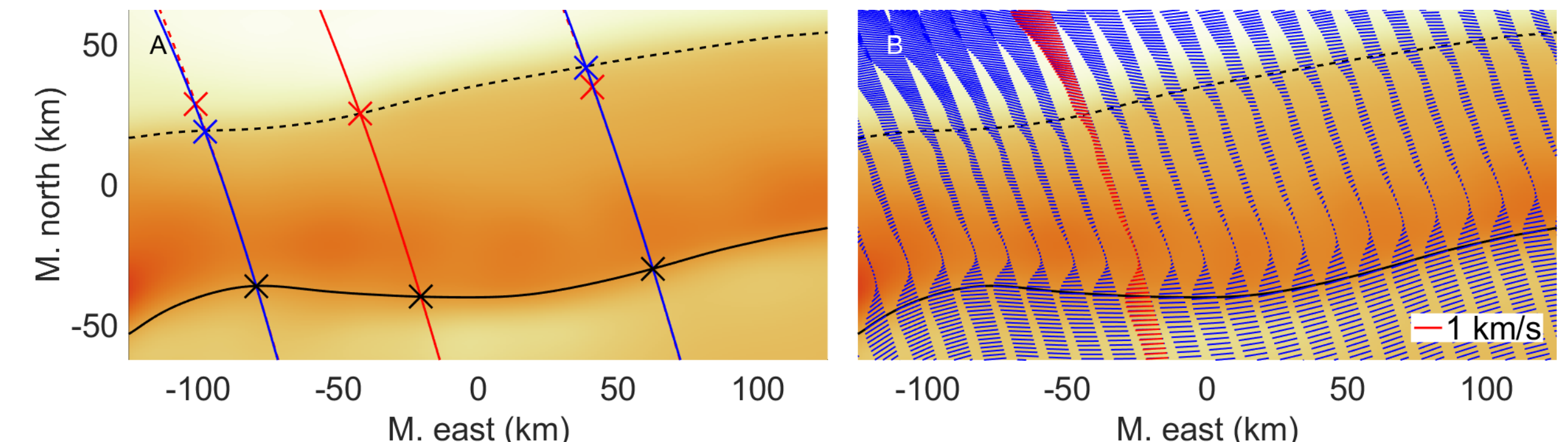
Figure 3: In situ flow data replication overlaid on the same conductance map from the left panel of Figure 2. A: Two replications (blue) of the original trajectory (red) along the primary arc boundary (solid black). The black crosses have the same flow data. The red/blue crosses indicate flow data before/after scaling. B: A low density replication (blue) along with the original, smoothed flow data (red).

Enforcing Electrostatic Flow

- After interpolating the replicated flow, we get the following associated electric field:

$$\mathbf{E}_i(x, y) = -\mathbf{v}_i(x, y) \times \mathbf{B} = -\nabla \phi(x, y) + \nabla \times \mathbf{A}(x, y) \quad (3)$$

- To enforce electrostatics, we minimize $\nabla \times \mathbf{A}$ which is done in one of two ways:
  1. **Brute force**: A least-squares fitting algorithm, in this case Levenberg-Marquart.
  2. **Helmholtz decomposition**: Using the Fourier transform method (Pers. Comm. A. Mule (2023)) by taking the dot product with $\mathbf{k}$ and the 2D FT of Eq. (3):

$$\mathbf{k} \cdot \mathbf{G}(k_x, k_y) = \mathbf{k} \cdot \left(-ik_x G_\phi(k_x, k_y) + i\mathbf{k} \times \mathbf{G}_A(k_x, k_y)\right) \Rightarrow G_\phi(k_x, k_y) = i(\mathbf{k} \cdot \mathbf{G})/\|\mathbf{k}\|^2 \quad (4)$$

- Giving $\phi_0(x, y) = \mathcal{F}^{-1}\{G_\phi(k_x, k_y)\}$, which is our potential up to a harmonic function.
- A generic polynomial harmonic function, f_m, of order m, where $\nabla^2 f_m = 0$, is fit to $\mathbf{E}_i$.
- The Helmholtz decomposition method takes several seconds whereas brute force fitting takes several hours, and they compare well (see Figure 4).
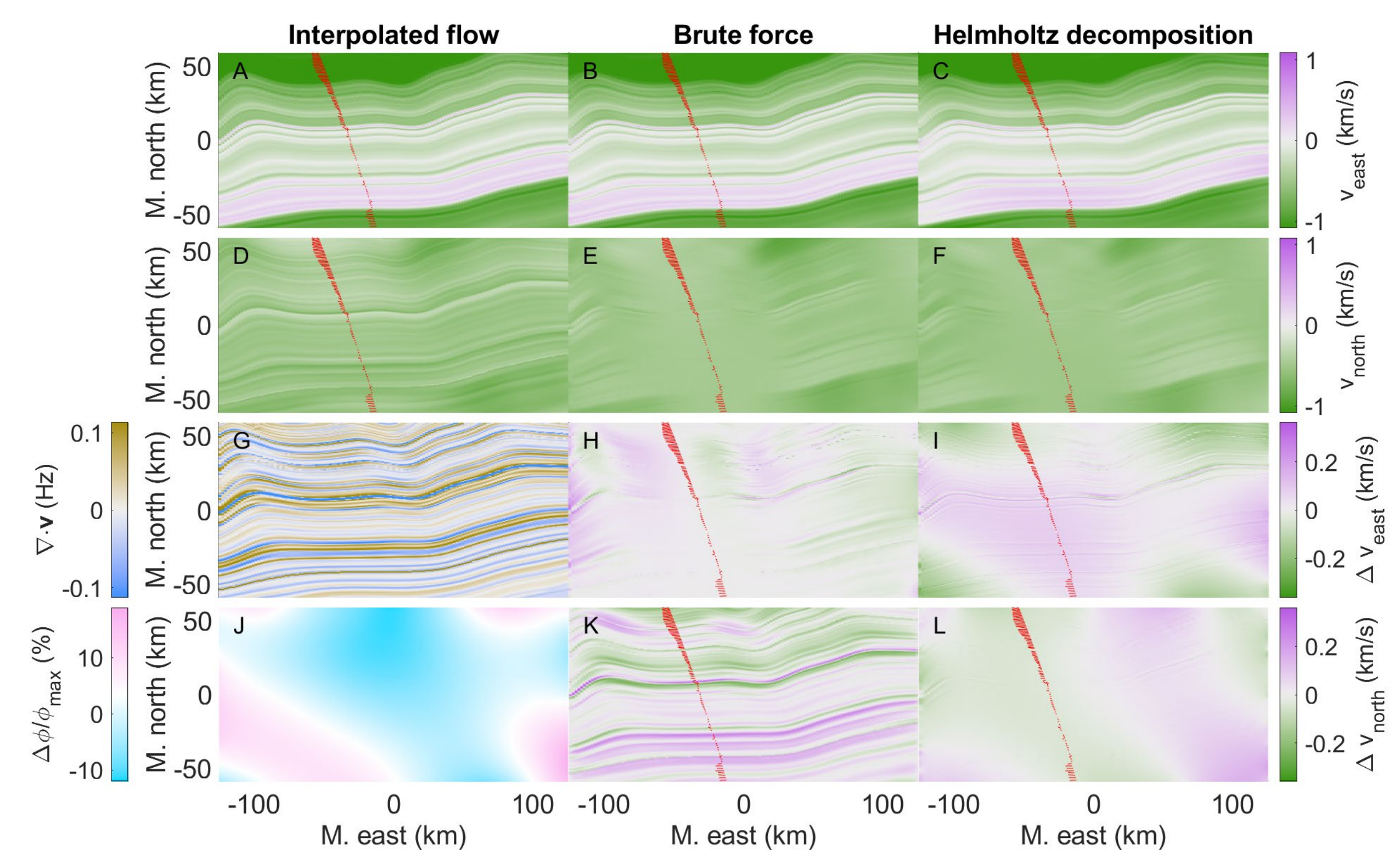
Figure 4: Comparison between fitting a potential map to an interpolated flow map. A-C: Eastward interpolated, brute force fitted, and Helmholtz decomposed flow. D-F: Same but northward. G: Divergence of the interpolated flow. H,K: Difference in east/northward flow between brute force and interpolated. I,L: Difference in east/northward flow between Helmholtz decomposed and brute force. J: Difference in potential between brute force and Helmholtz decomposed.

Replication Results

- Figure 5 shows final flow/potential maps with replication scaling/rotating on and off.
- With replication scaling, enhanced Σ_P is collocated with shorted out plasma flow.
- With replication rotating, the westward flow turns southward when the arc bends.
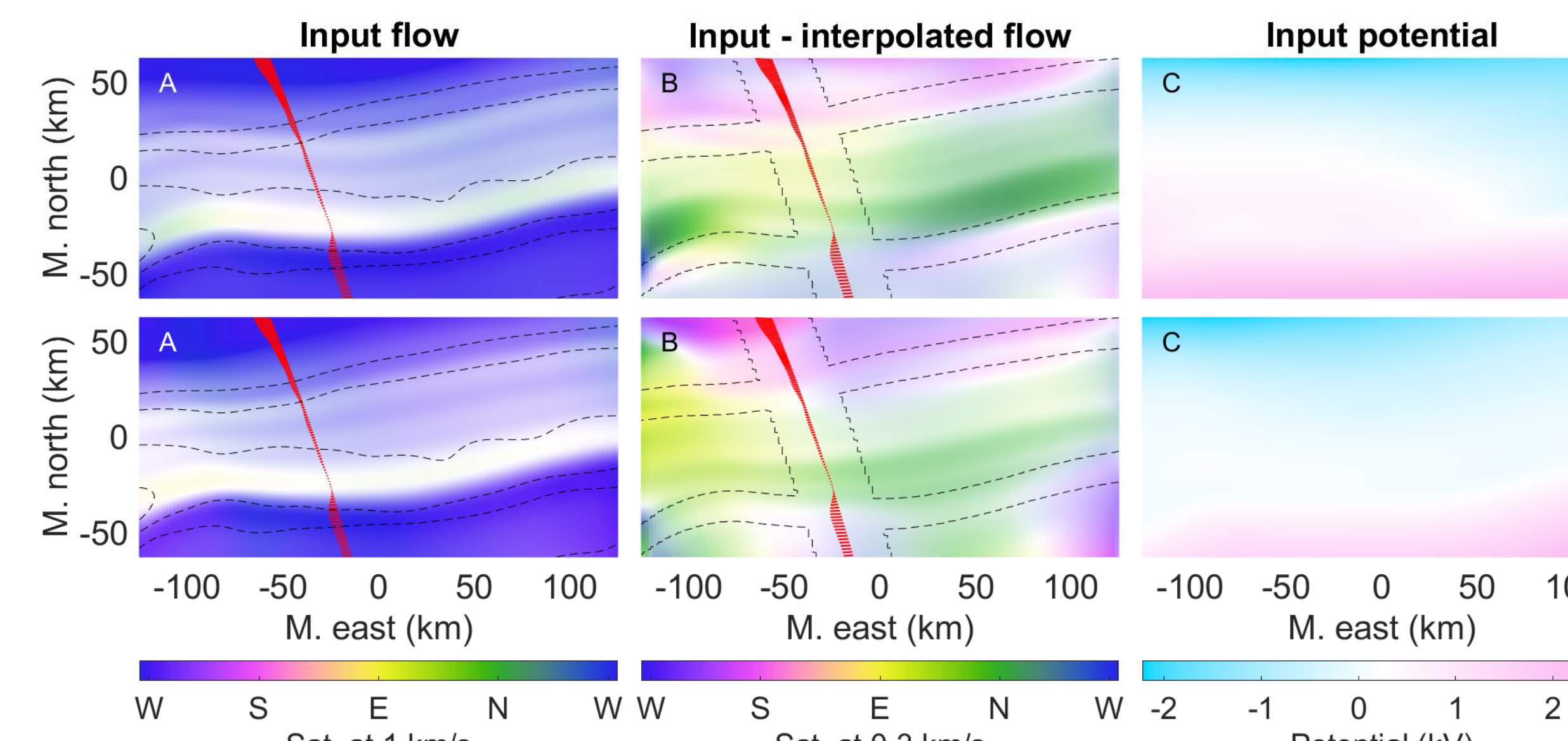
Figure 5: Input flow/potential maps used to drive simulations with (bottom row) and without (top row) replication scaling/rotating. A,D: Hue-saturation-value plot of $-\nabla\phi$ with contour lines of Σ_P. B,E: Flow error, i.e. $-\nabla\phi - \mathbf{v}_i$, with masking contours where the harmonic function is fit. C,F: Potential maps, ϕ.

Simulation Results

- To visualize 3D current closure, we use current flux tubes made possible by the condition of static current continuity, $\nabla \cdot \mathbf{j} = 0$, enforced by GEMINI.
- This simulation has background precipitation of 10 mW/m² at 1 keV, and arc precipitation that peaks at around 40 mW/m² at 9 keV.
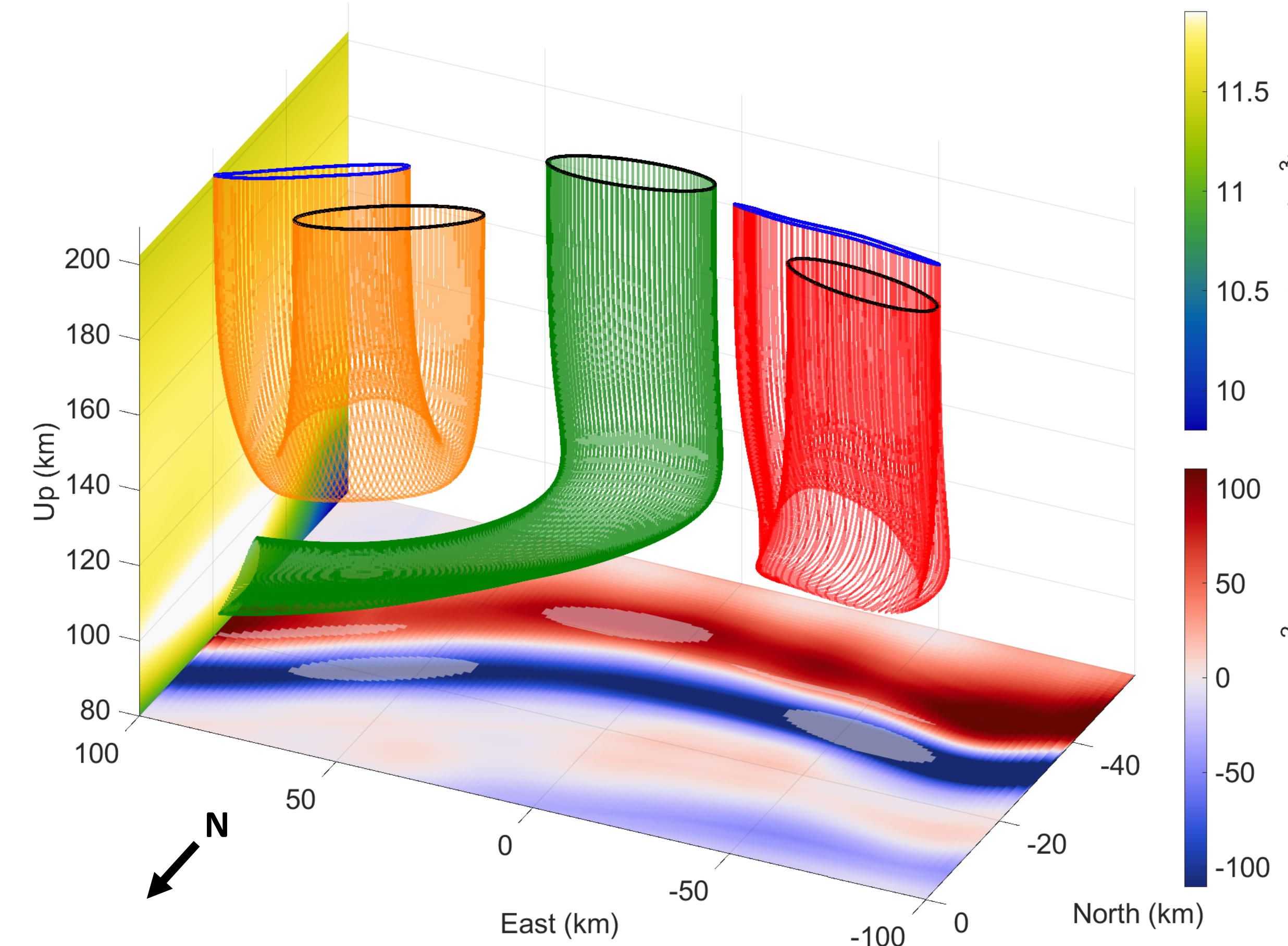
Figure 6: Isometric view (above) and top view (left) of the simulation results driven by flow from Figure 5. East wall: Electron density slice taken at 0 km east. Bottom: FAC slice taken at 200 km in altitude. Three fluxtubes are sourced at the black ellipses and terminate at the blue curves aside from the green one which terminates somewhere outside the model space.

Scan for videos of current flux tubes and more!

FAC Continuity Terms

- Figure 7 shows how the simulated FAC terms in Eq. (1) stack up against one another.
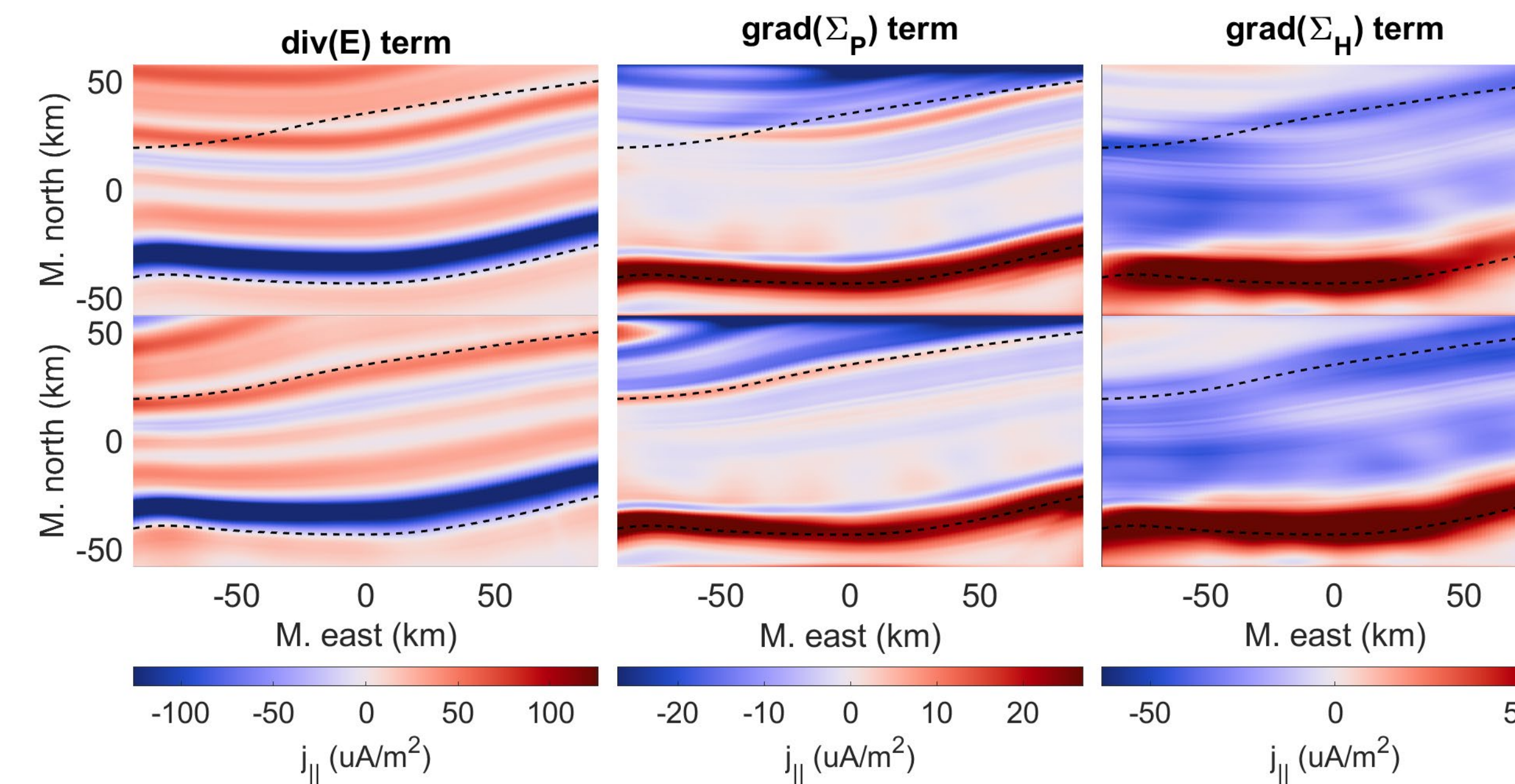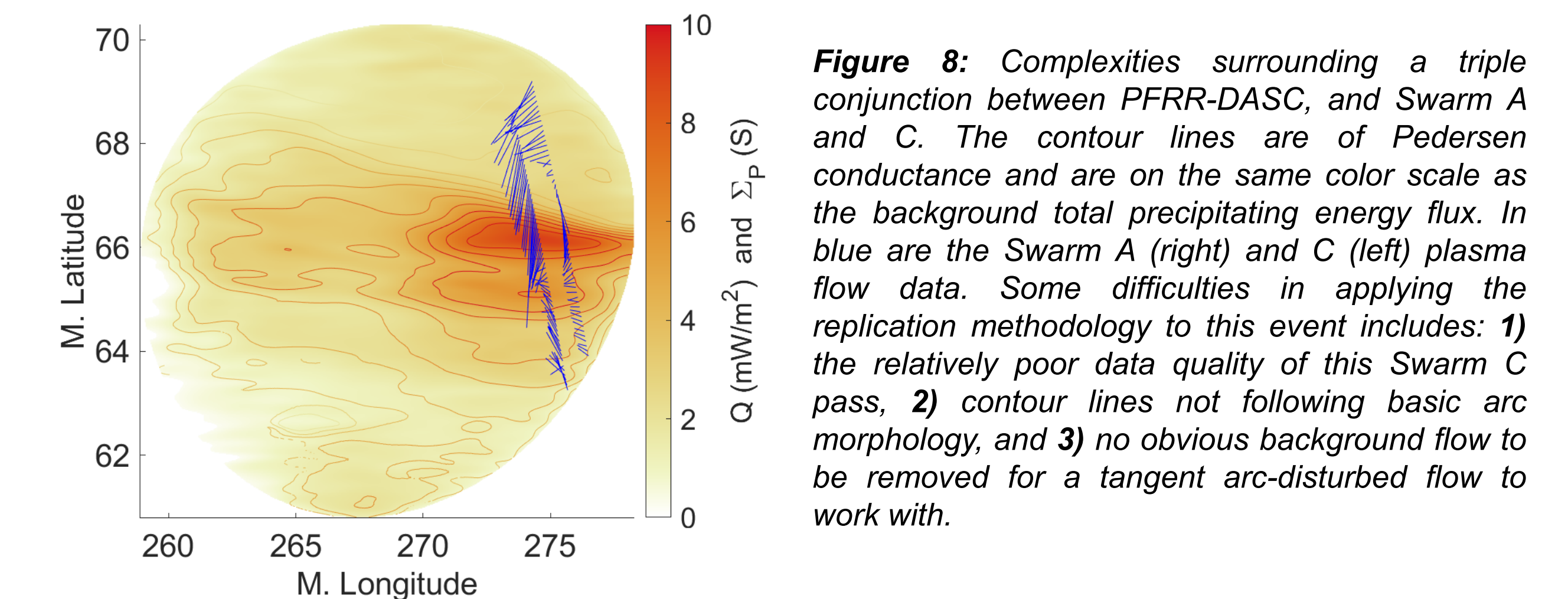- Note the deviating FAC intensity and morphology near the secondary boundary.

Figure 7: The three FAC terms from Eq. (1) with (bottom row) and without (top row) replication scaling/rotating. Dashed contours indicate the primary and secondary boundaries.

Discussions & Future Work

- For one of the most basic examples of an auroral system, the morphology of current closure is 3D in nature.
  - This is the interplay of the altitude-dependent Pedersen and Hall conductivities as current finds the path of least resistance.
- When driving 3D auroral simulations, maps of $\mathbf{v}$, Q, and E_0 (and ultimately $\Sigma_{P,H}$) need consistent smoothing, or low-pass filtering, in a way where the $\nabla \cdot \mathbf{E}$ term in Eq. (1) balances with the $\nabla\Sigma_{P,H}$ terms.
  - If the flow shear is too strong, the FAC might not find geophysical closure paths.
- Assuming $\nabla \cdot \mathbf{j} = 0$ and proper streamlines, if there is a mismatch in flux on either end of a current fluxtube, this can indicate a need for higher model resolution.
  - Doubling the altitudinal resolution improves influx/outflux ratios by a factor of 10.
- Interpolating scattered, replicated flow requires bicubic (or higher order) methods to avoid stepwise first derivates.
  - Bilinear interpolation can result in a strong rippling of simulated FAC.
- This methodology will be used to develop a hand-picked catalog of auroral simulations based on an existing list of conjunctions between ESA's Swarm spacecraft and all-sky, multi-spectral imagery from PFRR-DASC.
  - Figure 8 shows an example of a triple conjunction (Swarm A and C) and outlines further complexities in data driven 3D auroral simulations.

Figure 8: Complexities surrounding a triple conjunction between PFRR-DASC, and Swarm A and C. The contour lines are of Pedersen conductance and are on the same color scale as the background total precipitating energy flux. In blue are the Swarm A (right) and C (left) plasma flow data. Some difficulties in applying the replication methodology to this event includes: 1) the relatively poor data quality of this Swarm C pass, 2) contour lines not following basic arc morphology, and 3) no obvious background flow to be removed for a tangent arc-disturbed flow to work with.

Conclusions

- Even for the most basic auroral systems, a 2D description hides the 3D nature of current closure.
- When extrapolating plasma flow data surrounding auroral arcs, it is important to scale and rotate the data in accordance with conductance morphology.
- When data driving 3D auroral simulations, proper interpolation and model resolution are crucial.

Next up: A Catalog of Data 'Inspired' Simulations

- Ultimately, the methods outlined here are in aid of developing a catalog of both data driven simulations, but also more idealistic, data inspired simulations.
- More idealistic simulations will be used to do an auroral arc system sensitivity study to parameters such as:
  - Electron precipitation profiles (accelerated, Maxwellian, etc.)
  - FAC, flow, or precipitation intensities
  - Background electric fields
  - Basic arc morphology
- J. P. Dombeck has a list of FAST precipitation spectra ready and waiting for us!

References

Clayton, R. et al. (2019), *J. of Geophys. Research*, 10.1029/2018JA026440
Clayton, R. et al. (2021), *J. of Geophys. Research*, 10.1029/2021JA029749
Cowley, S. W. H. (2000), *Geophysical Monograph Series*, 10.1029/GM118p0091
Fang, X. et al. (2008), *J. of Geophys. Research*, 10.1029/2008JA013384
Kelley, M. C. et al. (2009), *Academic Press*, ISBN: 9780080916576
Khazanov, G. V. et al. (2018), *Space Weather*, 10.1029/2018SW001837
Laundal, K. M. et al. (2022), *J. of Geophys. Research*, 10.1029/2022JA030356
Lynch, K. A. et al. (2022), *J. of Geophys. Research*, 10.1029/2022JA030863
Marghitu, O. (2012), *Geophysical Monograph Series*, 10.1029/2011GM001189
Nicolls, M. J. et al. (2014), *Radio Science*, 10.1002/2014RS005519
Robinson, R. M. et al. (1987), *J. of Geophys. Research*, 10.1029/JA092iA03p02565
Sobel, I. (2014), *Pres. at Stanford A.I. Project 1968*, An Isotropic 3x3 Image Gradient Operator
Solomon, S. C. (2017), *J. of Geophys. Research*, 10.1002/2017JA024314
Wolf, R. A. (1975), *Space Science Reviews*, 10.1007/BF00718584
Zettergren, M. & Snively, J. (2019), *J. of Geophys. Research*, 10.1029/2018GL081569
Zettergren, M. & Semeter, J. (2012), *J. of Geophys. Research*, 10.1029/2012JA017637